



Investigation of Grinding and Lapping Surface Damage Evolution of Fused Silica by Inductively Coupled Plasma Etching

Zuocai Dai^{1,2,3} · Shanyong Chen^{1,2,3} · Xuhui Xie^{1,2,3} · Lin Zhou^{1,2,3}

Received: 7 January 2019 / Revised: 14 April 2019 / Accepted: 23 April 2019 / Published online: 6 May 2019
© Korean Society for Precision Engineering 2019

Abstract

Surface damage has great influence on optical properties, especially the laser-induced damage threshold of optics, and it has become a difficult and basic issue to find suitable methods to efficiently remove the surface damage for improving the surface quality. In this paper, the characteristic evolution of brittle scratch and ground/lapped surface damage during inductively coupled plasma etching (ICPE) process are experimentally investigated on fused silica. Results of damage removal tests show ICPE can efficiently remove brittle scratch and eliminate the lateral and medial cracks. The PV (peak to valley) and RMS (root mean square) values of surface roughness increase with the exposure of lateral and medial cracks, and then gradually decreases with further etching. Finally, the ground and lapped fused silica surfaces with a size of $300 \times 300 \times 20 \text{ mm}^3$ are efficiently processed by ICPE. The power spectral density analysis further demonstrates that the damage can be efficiently removed by ICPE. This study reveals the damage evolution during ICPE process and also provides technical guidance for optimizing the efficient damage removal process to rapidly improve surface quality, precision and fabrication efficiency of fused silica optics.

Keywords Inductively coupled plasma etching (ICPE) · Grinding and lapping damage · Fused silica

Abbreviations

ICPE	Inductively coupled plasma etching
SSD	Subsurface damage
MRF	Magnetorheological finishing
MRR	Material removal rate
HFE	Hydrofluoric acid etching
IBF	Ion beam figuring

1 Introduction

Fused silica material has been widely applied in modern optical systems such as the inertial confinement fusion facility and the ultraviolet lithography system, for its excellent optical properties [1]. However, in traditional fabrication of fused silica optics, the scratch, lateral and medial crack damages are inevitably produced during the grinding and lapping process [2]. Moreover, the post-processing for damage removal cannot yet meet the efficiency requirement of high performance optical systems [3]. These damages have a profound influence on the subsequent processes, and even affect the performance of fused silica optics such as the laser-induced damage threshold (LIDT) [4, 5]. In recent decades, it has become a difficult and basic issue to find suitable methods to efficiently remove conventional grinding and lapping damage for improving the surface quality of fused silica optics [2].

Conventional damage removal method is based on iterative lapping and polishing. By this way, it can successively reduce the thickness of damage layer, but cannot eliminate the damage thoroughly and efficiently [3, 6, 24]. Lately, various typical surface processing method such as magnetorheological finishing (MRF), hydrofluoric acid etching

✉ Shanyong Chen
mesychen@163.com

¹ College of Intelligent Science, National University of Defense Technology, 109 Deya Road, Changsha 410073, China

² Hunan Key Laboratory of Ultra-precision Machining Technology, Changsha 410073, Hunan, China

³ Laboratory of Science and Technology on Integrated Logistics Support, National University of Defense Technology, Changsha 410073, China

(HFE), ion beam figuring (IBF), and ICPE, have been used as the final polishing process to remove the damage generated during the previous process [4, 5, 12]. MRF can remove the damage defects, but Ce, Fe contamination in the MRF polishing fluid is always introduced to the subsurface, which seriously degrades LIDT [6]. HFE is regarded as a post-processing method for increasing the damage threshold by removing the subsurface damage (SSD) in hydrofluoric acid solution [7, 8]. However, continuous etching always leads to a decrease of damage threshold due to extended cracks, indentations, pits or scratches in geometrical structures [10]. IBF uses Ar^+ bombardment to remove material, which has the advantages of no contamination, non-contact pressure [9–11]. However, IBF can only remove the plastic scratches (at nanometer scale) and cannot effectively remove the brittle scratches (at micron scale), and its material removal rate (MRR) is very low [9, 12].

In contrast, ICPE using fluorine rich gases like NF_3 , CF_4 or SF_6 to produce active fluorine atoms achieves silicon based material removal in volatile fluorinated form of SiF_4 at atmospheric pressure [15]. The material removal type of ICPE is chemical etching without any mechanical or physical contribution, and no SSD appears [14]. Moreover, this chemical etching can achieve a very high MRR under appropriate conditions [15]. As a potentially efficient processing technology, ICPE has been studied by many researchers, such as plasma chemical vaporization machining (PCVM) proposed by Takino et al. [29], plasma jet machining (PJM) proposed by Arnold et al. [16–19], reactive atom plasma technology (RAPT) proposed by Fanara et al. [13, 20], and atmospheric pressure plasma polishing (APPP) proposed by Zhang et al. [21]. Recently Our research group proposed the arc-enhanced plasma machining (AEPM) [15]. These studies achieved high processing efficiency during ICPE, which demonstrated that ICPE could realize efficient processing of fused silica.

Nowadays, researchers are not only focused on the material removal efficiency of ICPE, but also show great concern on surface quality and the mechanism of morphology evolution during ICPE process. Zhang et al. recently showed through simulation that for actual macro-scale surface with millions of atoms, convex morphology could be eliminated faster than concave one [21, 31, 32]. Wang et al. had reported that the vanishing of sharp points formed in pits coalescing owed to the side wall etching of the pits [27, 30, 33]. Accordingly, details in the lateral and medial crack damage morphology evolution with efficient removal of the grinding and lapping damage at micron scale during ICPE process are rarely shown. It is not yet clear how this damage morphology changes during ICPE process compared with contact damage removal approach such as MRF, and how to efficiently utilize ICPE to remove the grinding and lapping damage. The answers to these questions will make a

great sense for understanding the influence law of grinding and lapping damage evolution during ICPE process and optimizing the damage efficient removal process of fused silica optics.

This study was conducted to focus on the morphology evolution with efficient removal of the scratch, lateral and medial cracks on the ground and lapped fused silica samples during ICPE process. Multiple characterization results of ICPE etched scratch, ground and lapped surfaces are shown, respectively. Results systematically reveal the damage morphology evolution law during ICPE process and also could provide technical guidance for optimization of the grinding and lapping damage removal process for fused silica optics.

Assessment of surface morphology was performed by means of digital microscope (Keyence VHX-600E). The removal depth and PV value were measured by Taylor profilometer (Talysurf PGI 1240). The sample surface form was measured by coordinate measuring machine (Zeiss ACC URA) and 24-in. large aperture wavefront interferometer (Zygo VeriFire MST).

2 Experiment Preparation

Six fused silica samples (#1, #2, #3, #4, #5 and #6) with a size of $100 \times 100 \times 10 \text{ mm}^3$ are used to investigate the damage morphology evolution during ICPE process. The sample #7 and #8 with a size of $300 \times 300 \times 20 \text{ mm}^3$ are used to observe the surface evolution when removing the ground and lapped damage by ICPE, respectively.

The processing parameters shown in Table 1 are used to etch the samples #1, #2, #5 and #6, while the processing parameters for the samples #7 and #8 are based on the actual damage conditions. The samples are processed in the ICPE system developed by our research group. Figure 1a shows the plasma source structure and Fig. 1b shows the processing system.

As shown in Fig. 1b, the plasma processing experiment is based on the material removal footprint. When the parameters of gas flow, target distance and tool-path are determined, different removal depth can be achieved by the scanning rate of the plasma beam. The material removal

Table 1 Table of processing parameters of ICPE

Item	Level
Inner tube	SF_6 30 sccm and Ar 15 sccm
Intermediate tube	Ar 1.12 slm
Outer tube	Ar 16.8 slm
Stand-off distance between Laval-nozzle and sample	5 mm
Tool-path	Reversed staggered raster path

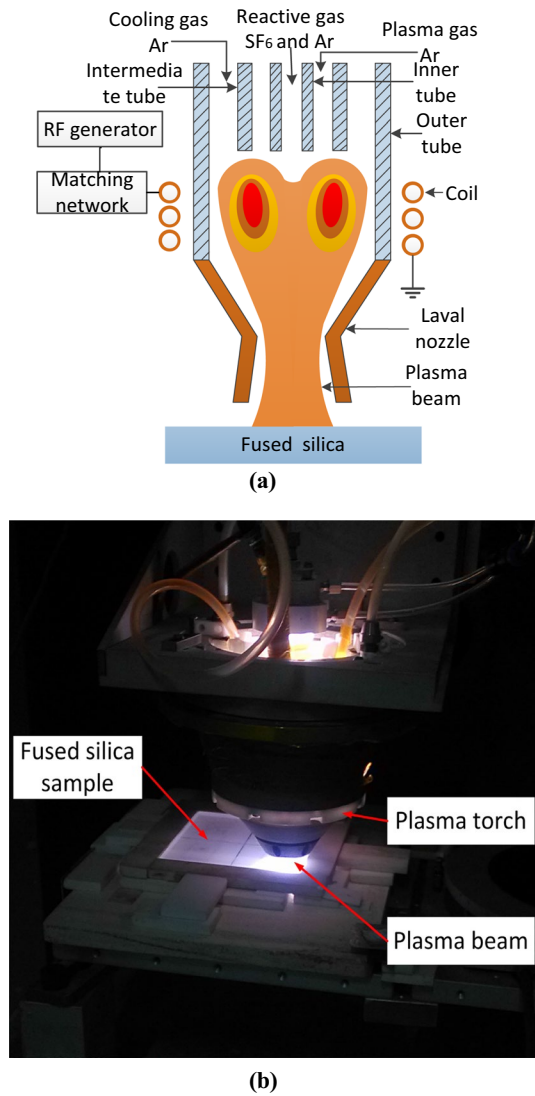


Fig. 1 ICPE system: **a** plasma source structure, **b** processing status

depth is measured approximately at the same location before and after plasma etching by the Taylor profilometer, then the section profiles are obtained by data fitting. Meanwhile the removal profile can be obtained through subtracting the initial surface by the processed surface.

The samples #1 and #2 are used to evaluate the scratch morphology evolution during plasma etching. A further quantitative study on the damage removal process is taken on two different kinds of scratch (single scratch and cross scratches). The scratches are produced by Ultra Nano-indentation Tester with Rockwell pressure diamond head on the conventional polished samples. As shown in Fig. 2a, the single scratch was produced by 1.5 N loading forces. As shown in Fig. 3a, the horizontal and vertical scratches are produced by 2.5 N and 3.5 N loading forces, respectively.

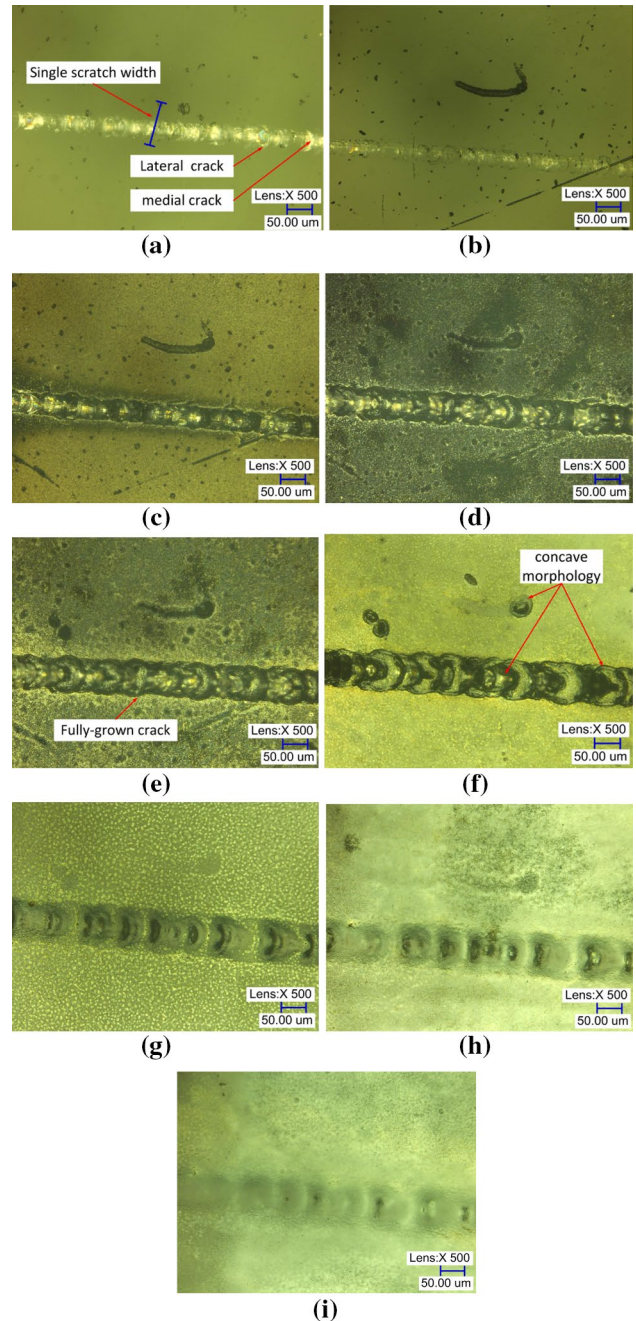


Fig. 2 Evolution of single scratch ($\times 500$ magnification) on the sample #1 during ICPE process at different depths: **a** 0 μm , **b** 3.2 μm ; **c** 6.5 μm , **d** 9.2 μm , **e** 18.6 μm , **f** 32.9 μm , **g** 44.5 μm , **h** 52.6 μm , **i** 61.5 μm removal depth. Image size is 610 μm (length) \times 450 μm (width)

The samples #3 and #4 are used to test the grinding and lapping damage distribution at different removal depths during MRF process, respectively. The samples #5 and #6 are used to observe the morphology evolution of the ground and lapped surface during ICPE process, respectively. The samples #3 and #5 are ground by

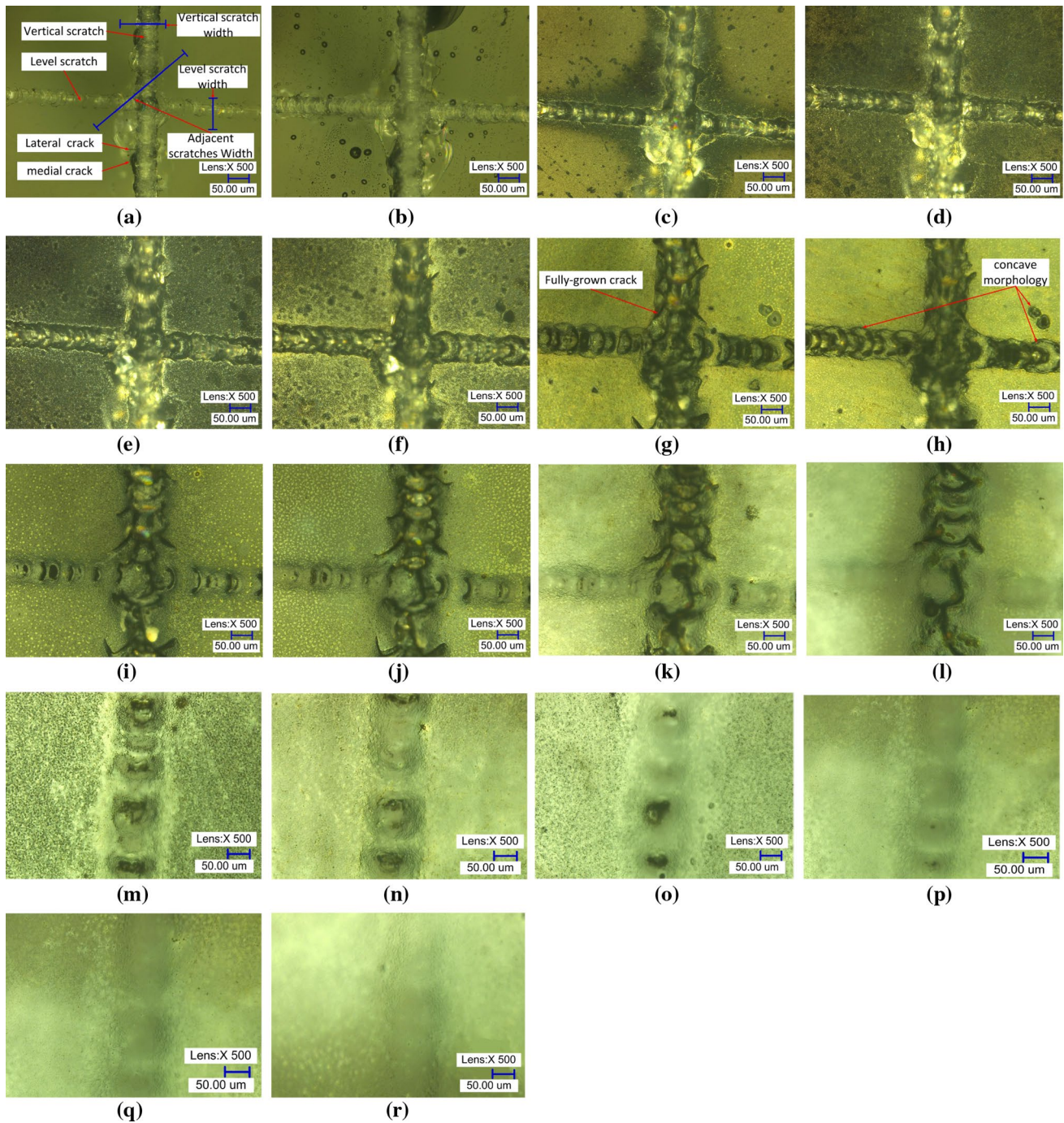


Fig. 3 Evolution of cross scratches ($\times 500$ magnification) on the sample #2 during ICPE process at different removal depths, **a** 0 μm , **b** 3.1 μm , **c** 6.4 μm , **d** 9.8 μm , **e** 12.8 μm , **f** 18.5 μm , **g** 24.9 μm , **h**

31.5 μm , **i** 37.3 μm , **j** 44.9 μm , **k** 51.2 μm , **l** 60.2 μm , **m** 68.6 μm , **n** 75.8 μm , **o** 79.5 μm , **p** 84.8 μm , **q** 92.2 μm , **r** 100.6 μm removal depth. Image size is 610 μm (length) \times 450 μm (width)

a cross-grinding machine. Typical grinding damage is produced in the cross-grinding process (120 grit grinding, cutting speed = 2500 rpm, feed rate = 8 mm/s, depth of cut = 30 μm) [22]. The samples #4 and #6 are processed by the lapping process (relative speed = 2 m/s, pressure = 2.7 kPa) for 30 min, and the lapping slurry

consists of 20 grit (20 μm) diamond abrasives and water in a volume ratio of 1:20, in order to obtain the typical lapping damage [2].

3 Scratch Evolution Test During ICPE Process

3.1 Results

Figures 2 and 3 show scratch removal results at different removal depths. As shown in Fig. 2, single scratch damage is firstly exposed, gradually developed to fully-grown scratch, and then extended to concave morphology. It is finally smoothed with the increase of removal depth by ICPE. As shown in Fig. 3, the cross scratch damage is also revealed, and then gradually removed by ICPE. Meanwhile, the adjacent area of cross scratches is gradually merged together through chemical isotropic etching after the formation of the fully-grown scratch [28].

3.2 Analysis

The profile measurement mode of digital microscope is used to measure the scratch profile at different removal depths. Scratch profiles in Fig. 4a–c are corresponding to the single scratch in Fig. 2, the horizontal scratch and the vertical scratch in Fig. 3, respectively. Variations of these scratch profiles at different removal depths also present the morphology evolution of the damage generated by different loading forces. As shown in Fig. 4a, the initial depth of the scratch is about $0.8\ \mu\text{m}$ and width is $33.2\ \mu\text{m}$, and there are obvious lateral and medial cracks around the scratch in the field of view in Figs. 2a and 3a. However, at the removal depth of $3.2\ \mu\text{m}$, the scratch gets wider and deeper with the exposure of lateral and medial cracks. The scratch depth gradually increases from 2.7 to $7.2\ \mu\text{m}$. The lateral and medial cracks develop to the fully-grown cracks at the removal depth of $18.6\ \mu\text{m}$. The crack damages develop to concave morphologies, and then the concave morphologies gradually get shallow with further etching. The scratch depth decreases from 7.2 to $2.3\ \mu\text{m}$ (Fig. 2i) and width is $61.5\ \mu\text{m}$. The evolution law of the cross scratches at different removal depths is consistent with that of the single scratch, which verifies the damage morphology evolution law. Previous researches have confirmed that the convex morphology is removed faster than the concave one, and then the sample surface is gradually smoothed during ICPE process [21]. Figure 4d shows how the two adjacent scratches evolve. Two adjacent scratches firstly become the concave morphologies (valleys) with the increase of removal depth. Next the convex morphology (saddle) between the two valleys becomes narrow. Then two adjacent scratches are merged together, and the scratch depth approaches the original depth ($1.5\ \mu\text{m}$, Fig. 3l). Finally, the two adjacent scratches are fully merged together, which would make the sample surface smoother. As the walls of

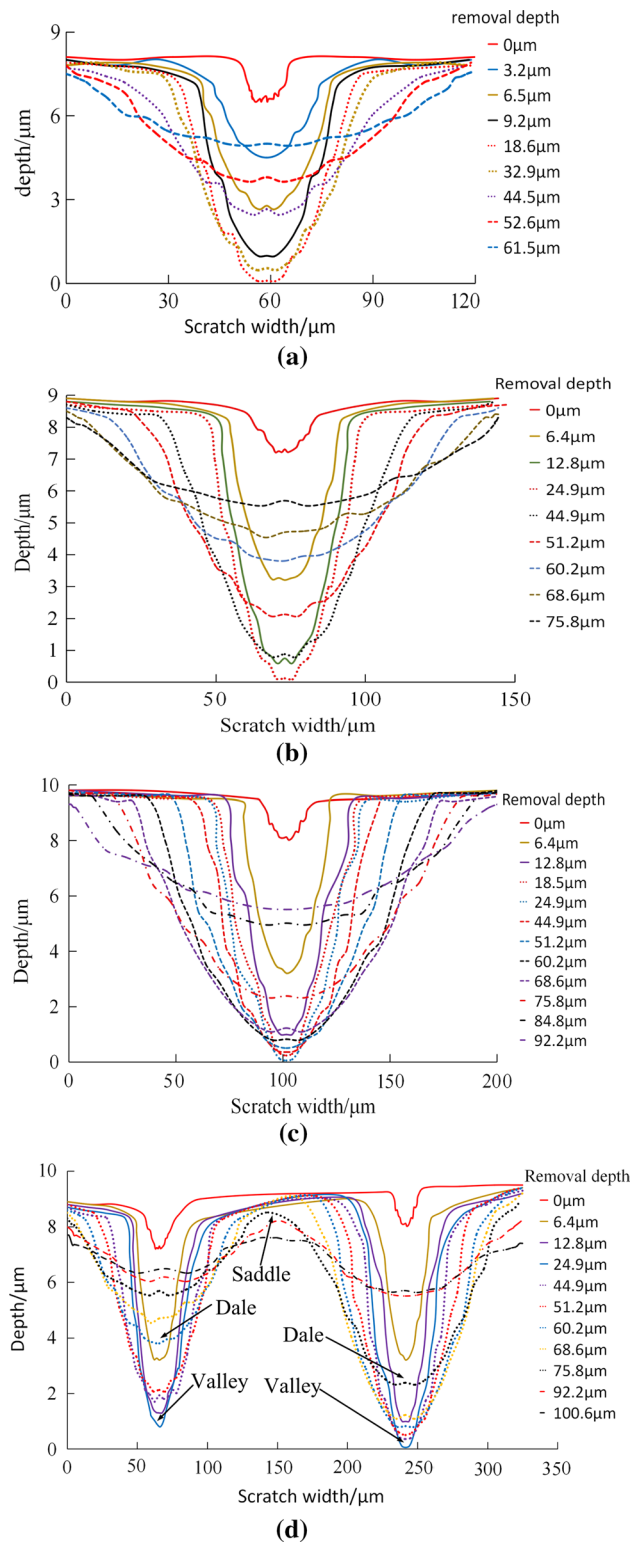


Fig. 4 Scratch profile micro-structures evolution in different ICPE removal depths: **a** single scratch (1.5 N loading forces), **b** horizontal scratch of cross scratches (2.5 N loading forces), **c** vertical scratch of cross scratches (3.5 N loading forces), **d** adjacent scratches of cross scratches

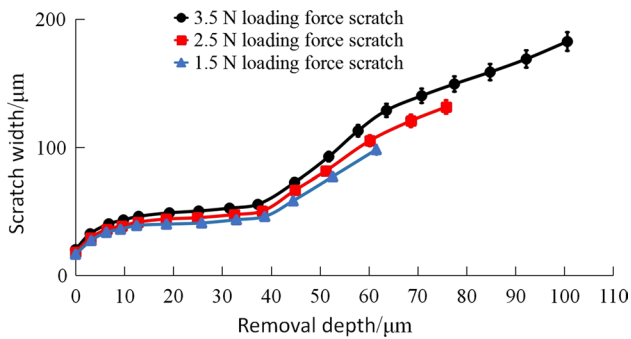


Fig. 5 Scratch width variation with removal depth

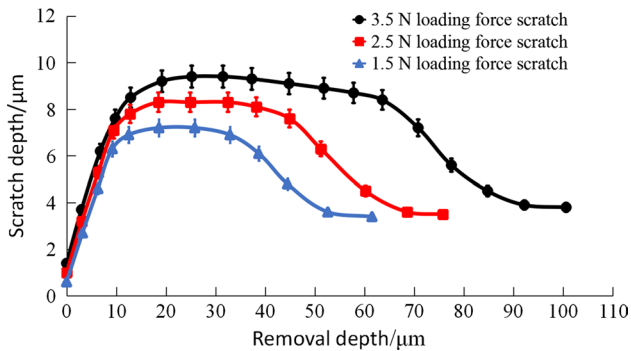


Fig. 6 Scratch depth variation with removal depth

the valleys are etched by chemical active particles, such saddle between the two valleys gradually develops to the dales with the increase of the removal depth. This property of isotropic etching creates a special connectivity with the adjacent dale, which may share a wall of another adjacent dale where the active particles etch. Finally, the surface morphology gradually tends to be flat (Fig. 4d).

To further investigate the scratch damage produced at different loading forces, the analysis for the scratch width, depth and width–depth ratio is carried out at different removal depths. Figure 5 shows that scratch widths of the loading forces consistently increase with the increase of removal depth, and the bigger loading force will cause the wider scratch. Figure 6 shows the variation of scratch depth at different removal depths. Obviously, scratch depths firstly increase with the increase of removal depth, and the maximum value appears at the situation of the full development of lateral and medial cracks, then decreases to a value close to the original scratch depth with the extension of the valley. Figure 7 shows the variation of the scratch width–depth ratio at different removal depths. It is very clear that the width–depth ratio firstly decreases with the increase of removal depth, and the minimum value appears at the point of the maximum depth of the valley. Then the width–depth ratio increases sharply with

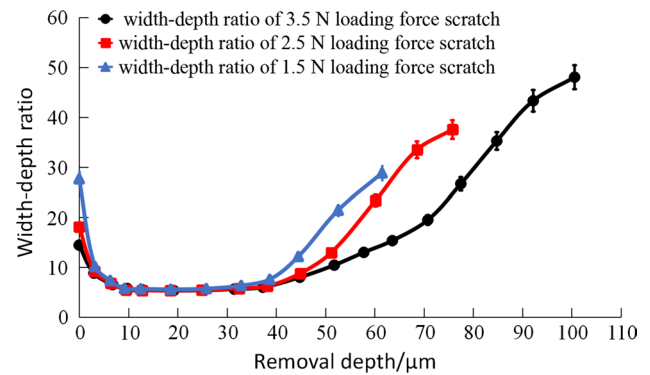


Fig. 7 Scratch width–depth ratio variation with removal depth

increase of removal depth, which displays that the width of the valley is quickly getting wider. As we known, the etched surfaces are supposed to be flat and uniform, yet plasma etching usually makes the scratch develop at depth in the initial processing phase and then be smoothed with further chemical isotropic etching. All those variation laws of the scratches produced by different loading forces fully demonstrate the plasma etching as a good processing way of efficiently smoothing the brittle scratch.

4 Grinding and Lapping Damage Distribution Test

4.1 Damage Depth Test

In order to acquire the damage distribution for evaluating the etching behavior of ICPE process, we first use MRF spot technique [22] to test the damage distribution with the samples #3 and #4. The sample #3 is used to test the ground surface, while the sample #4 is used for lapped surface test.

As shown in Fig. 8, the crack damage produced in grinding process is obvious and can be classified into two types, lateral and medial cracks (Fig. 8b). As the increase of removal depth, the redeposition products decrease and the density of lateral and medial cracks gradually appear clearly in the range of 0–7.6 μm under the surface. Then the cracks are gradually reduced with the removal depth ranging from 10 to 59.2 μm . Finally, the cracks vanish completely on the surface when the removal depth is above 59.2 μm .

As shown in Fig. 9, typical damage is generated during a 20 grit lapping process in different depths. The cracks are slight and uniform compared to grinding damage, and these cracks decrease with the increase of removal depth. Finally, the crack damages disappear and the undamaged surface appear when the removal depth reaches above 28.8 μm .

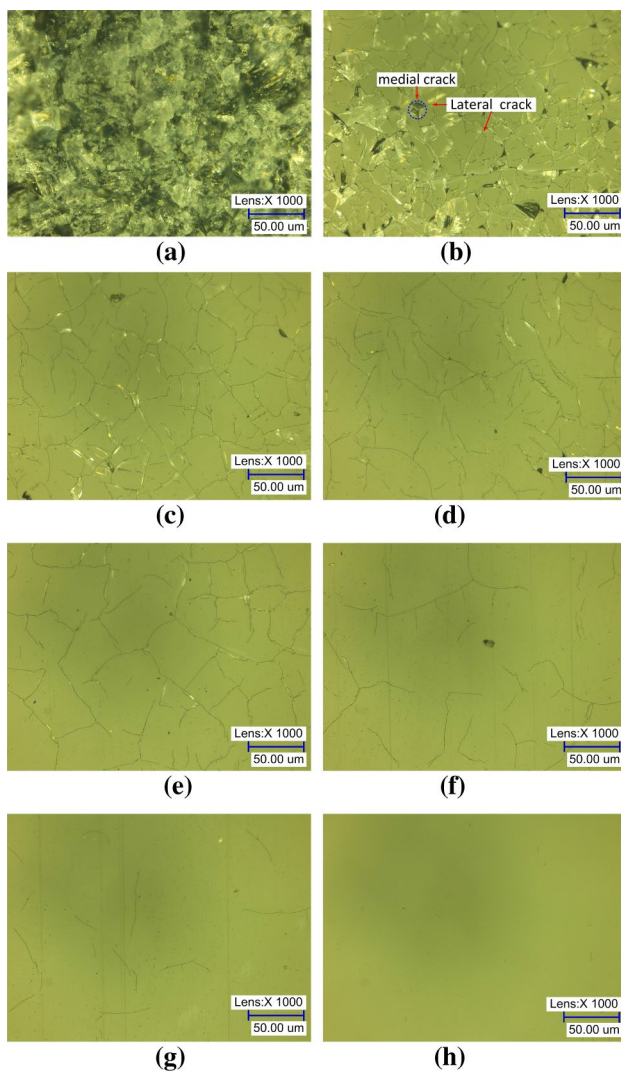


Fig. 8 Grinding damage ($\times 1000$ magnification) evolution on the sample #3 at different removal depths by MRF: **a** 0 μm , **b** 7.6 μm , **c** 15.2 μm , **d** 22.9 μm , **e** 32.5 μm , **f** 40.3 μm , **g** 48.6 μm , **h** 59.2 μm under the surface. Image size is 308 μm (length) \times 230 μm (width)

4.2 Damage Distribution During ICPE Process

The grinding and lapping damage distribution is shown in Figs. 10 and 11, respectively. As shown in Fig. 10, the PV value increases with the increase of removal depth, and the maximum of 15.6 μm appears at the removal depth of 25.9 μm , then decreases to the minimum of 3.2 μm at the removal depth of 62.6 μm . While for lapping damage, Fig. 11 shows that the PV value rapidly increases to the maximum of 8.3 μm at the removal depth of 12.8 μm , then decreases to the minimum of 1.5 μm at the removal depth of 25.6 μm . These results not only verify the maximum depth of the damage, but also reveal that both of the grinding and lapping damage is gradually exposed and then eliminated during ICPE process. In these processes, the redeposition

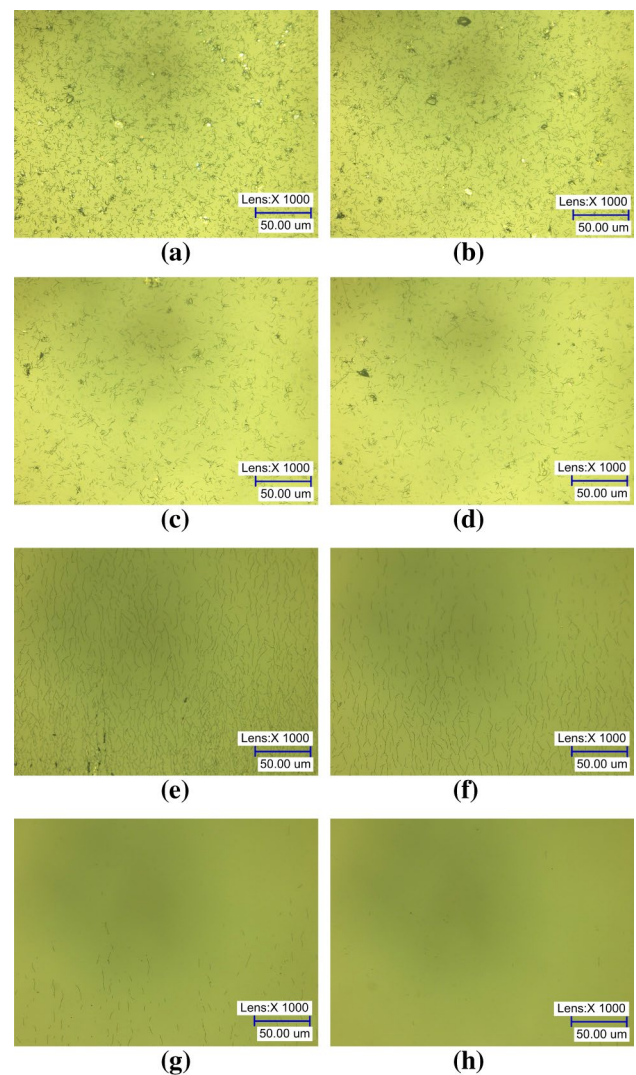


Fig. 9 Lapping damage ($\times 1000$ magnification) evolution on the sample #4 at different removal depths by MRF: **a** 0 μm ; **b** 2.9 μm ; **c** 6.7 μm ; **d** 10.6 μm ; **e** 16.3 μm ; **f** 19.8 μm ; **g** 24.3 μm ; **h** 28.8 μm under the surface. Image size is 308 μm (length) \times 230 μm (width)

products are gradually removed, and then the lateral and medial cracks are exposed and develop to the fully-grown concave morphology. These processes cause increase of the PV value with the increase of removal depth. Next, the fully-grown concave morphologies are extended in the width for the plasma etching, which causes decrease of the PV value. All those results demonstrate ICPE can eliminate the lateral and medial cracks and does not bring in the mechanical contact residual stress damage.

According to surface damage evolution during ICPE process, the damage removal procedure can be described as a series of morphology evolution processes. Figure 12 shows that the brittle damage morphology profile evolution and the detail processes can be described as following steps. Firstly, surface redeposition products generated in

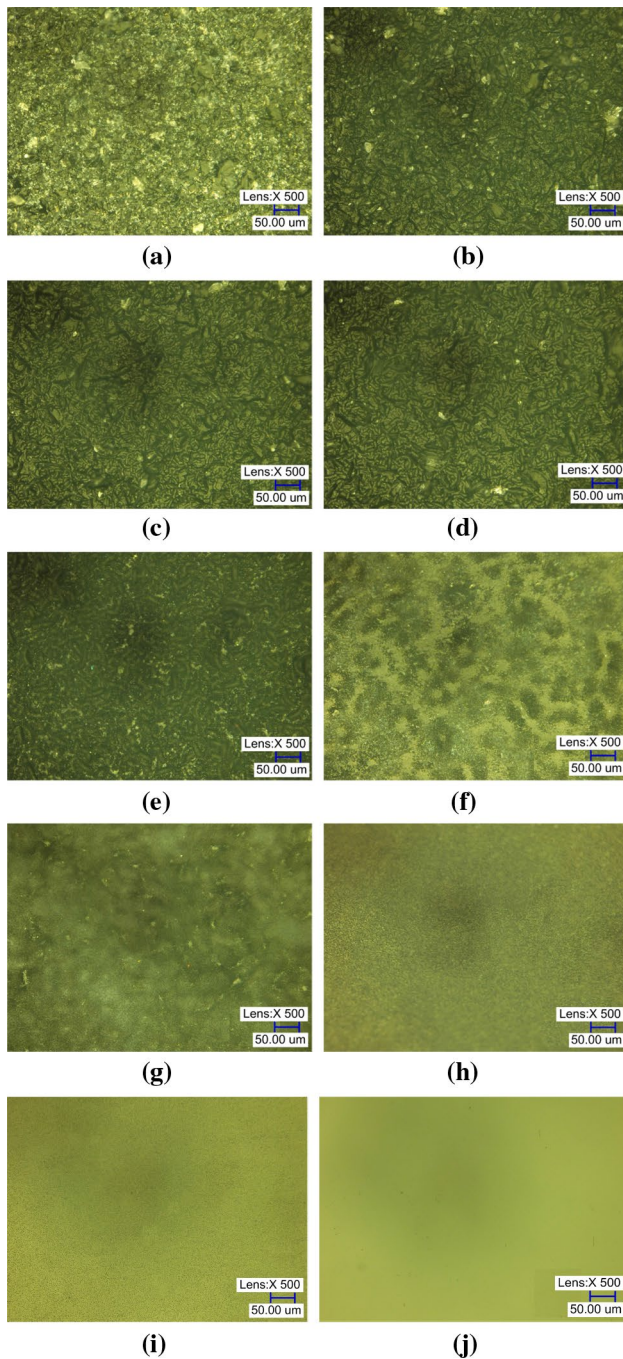


Fig. 10 Grinding damage morphologies ($\times 500$ magnification) evolution on the sample #5 during ICPE process at different removal depths: **a** 0 μm , $\text{PV}=6.8 \mu\text{m}$; **b** 1.8 μm , $\text{PV}=8.7 \mu\text{m}$; **c** 5.6 μm , $\text{PV}=10.9 \mu\text{m}$; **d** 15.7 μm , $\text{PV}=14.2 \mu\text{m}$; **e** 19.6 μm , $\text{PV}=15.1 \mu\text{m}$; **f** 25.9 μm , $\text{PV}=15.6 \mu\text{m}$; **g** 39.3 μm , $\text{PV}=9.3 \mu\text{m}$; **h** 44.5 μm , $\text{PV}=6.7 \mu\text{m}$; **i** 52.6 μm , $\text{PV}=4.6 \mu\text{m}$; **j** 62.6 μm , $\text{PV}=3.2 \mu\text{m}$. Image size is 610 μm (length) \times 450 μm (width)

grinding and lapping process are removed by the plasma etching, which causes exposure of the medial and the lateral cracks on the surface. Secondly, the medial cracks extend to the interior of a fused silica substrate, and the

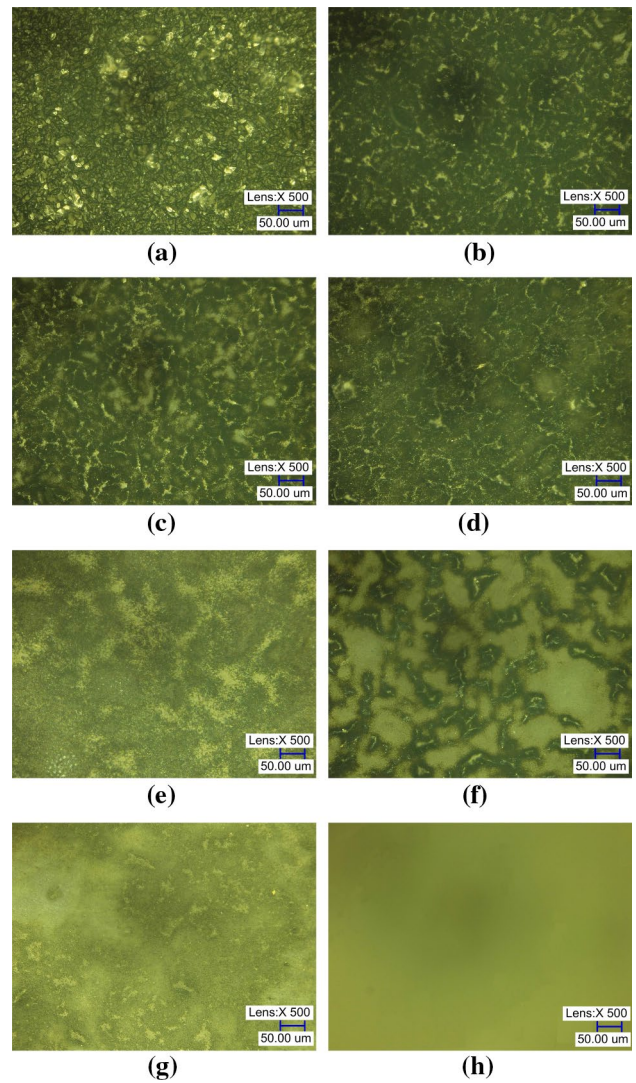


Fig. 11 Lapping damage morphologies ($\times 500$ magnification) evolution on the sample #6 during ICPE process at different removal depths: **a** 0 μm , $\text{PV}=1.9 \mu\text{m}$; **b** 1.2 μm , $\text{PV}=3.2 \mu\text{m}$; **c** 6.3 μm , $\text{PV}=6.2 \mu\text{m}$; **d** 9.9 μm , $\text{PV}=7.8 \mu\text{m}$; **e** 12.8 μm , $\text{PV}=8.3 \mu\text{m}$; **f** 15.5 μm , $\text{PV}=6.9 \mu\text{m}$; **g** 18.6 μm , $\text{PV}=3.8 \mu\text{m}$; **h** 25.6 μm , $\text{PV}=1.5 \mu\text{m}$. Image size is 610 μm (length) \times 450 μm (width)

lateral cracks extend around the medial cracks, developing to fully-grown cracks because of plasma chemical isotropic etching. Such etching leads to undercuts in the crack layer, and thus increases the effective width of the crack. Thirdly, the fully-grown cracks extend to form the valley for morphology duplicate etching [28]. Fourthly, the single valley develops to dales, and gradually the adjacent dales merge together [21]. Finally, the surface is gradually smoothed by plasma etching and tends to be flat.

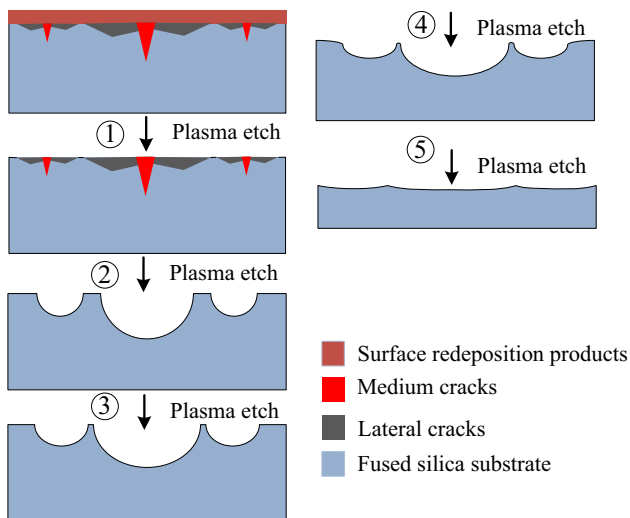


Fig. 12 Damage morphology evolution during ICPE process

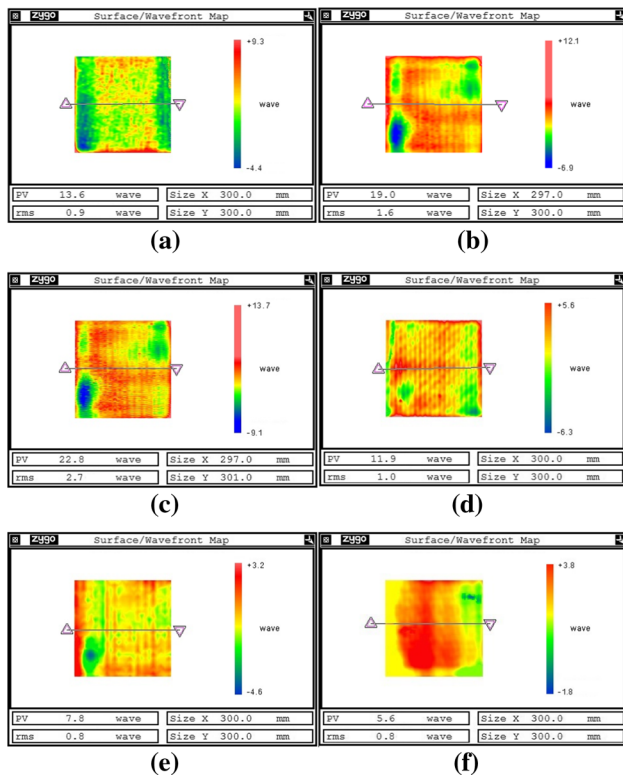


Fig. 13 Ground surface error evolution on the sample #7 during ICPE process at: a 0 μm , b 11.3 μm , c 24.6 μm , d 36.3 μm , e 49.8 μm , f 61.7 μm removal depth

5 Efficient Processing of Ground and Lapped Surface Using ICPE

The surfaces in Figs. 13 and 14a–d are measured by the

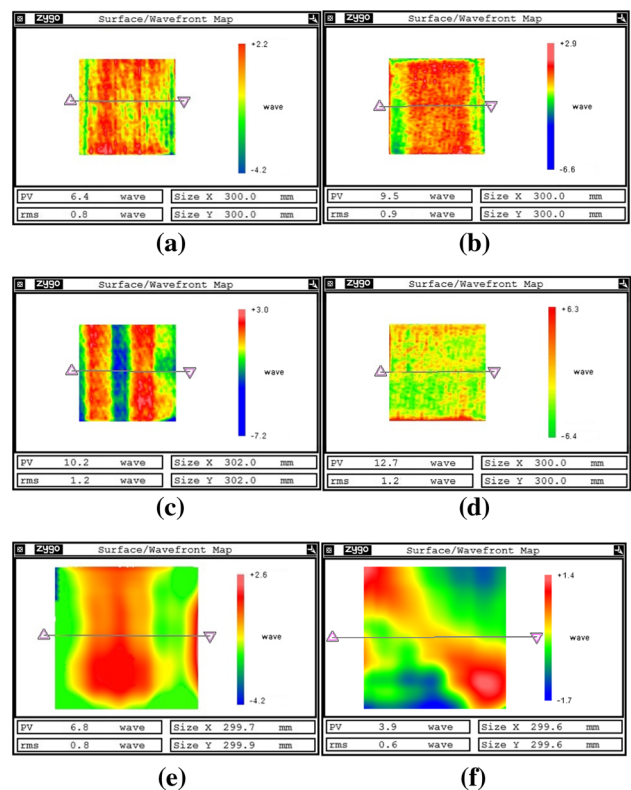


Fig. 14 Lapped surface evolution on the sample #8 during ICPE process at: a 0 μm , b 5.2 μm , c 10.7 μm , d 16.8 μm , e 22.6 μm , f 28.5 μm removal depth

coordinate measuring machine. For the convenience of data analysis, the data are converted into Binary Data File supported by Zygo MetroPro software. The surfaces in Fig. 14e, f are measured by 24-in. large aperture wavefront interferometer.

Figures 13 and 14 show the form error evolution of ground and lapped surfaces during ICPE process, respectively. Considering the grinding damage distribution in Sect. 4, processing with 200 mm/min scanning rate is performed, and the MRR could be as high as 6.5 mm³/min. While for lapped surface, 400 mm/min scanning rate is used, and the MRR could reach 4.6 mm³/min. Figure 13 shows the ground surface error ($\lambda = 632.8 \text{ nm}$ is the wavelength of the wavefront interferometer) at different removal depth. The surface error increases from the initial value of 13.6 λ PV 0.9 λ RMS (Fig. 13a) to the maximum value of 22.8 λ PV 2.7 λ RMS (Fig. 13c) at the removal depth of 24.6 μm , then the PV value decreases to 5.6 λ PV 0.8 λ RMS (Fig. 13f) with the increase of removal depth. As shown in Fig. 14, the lapped surface error firstly increases from the initial value of 6.4 λ PV 0.8 λ RMS (Fig. 14a) to the maximum value of 12.7 λ PV 1.2 λ RMS (Fig. 14d) at the removal depth of 16.8 μm , then decreases to 3.9 λ PV 0.6 λ RMS (Fig. 14f). These results demonstrate ICPE can efficiently

remove the grinding and lapping damage while reducing the surface error simultaneously under appropriate processing conditions.

6 Discussion

Three issues concerned in this paper are discussed as below:

- (1) Evolution of the damage during ICPE process. Firstly, ICPE can efficiently smooth the micro-morphology defects of brittle scratches and can effectively remove the lateral and medial cracks produced by mechanical contact residual stress. Thus, ICPE can result in a significant reduction of defects in fused silica surface with its chemical etching (Figs. 2, 3, 10, 11). Secondly, profile evolution of the scratches at different removal depths demonstrates ICPE can effectively smooth the concave morphology (Fig. 2f, 3h) evolved from the scratch (Fig. 4). Moreover, the width, depth and width–depth ratio variation analysis of the scratches verifies that ICPE can efficiently eliminate the scratches on fused silica surface (Figs. 5, 6, 7). Thus, the instinctive fused silica surface can be processed without mechanical residual stress defects.
- (2) Increase mechanism of surface error and PSD analysis during ICPE process. The surface error is further reduced with the continuous ICPE, and the value of surface error appears to increase or be even much bigger than the original surface error in the initial ICPE phase (Figs. 13a–c, 14a–d). It is because chemical isotropic etching induces exposure of lateral and medial cracks, then the exposed cracks develop to fully-grown cracks, and finally the grown cracks gradually form the concave morphologies with further etching [22]. These processes lead to the increase of the surface error. Afterwards the value of surface error gradually decreases with the concave morphologies smoothed (Figs. 13d–f, 14e–f).

In comparison, MRF as another damage removal approach removes the damage through free abrasive with a contact mechanical polishing wheel and magnetization [24]. Figure 15a shows that the PV roughness value gradually reduces during MRF process [3, 23], while for ICPE, Fig. 15b shows that the PV roughness value firstly increases, and then gradually decreases, so the instinctive fused silica surface appears. It is because chemical isotropic etching causes removal of the exposed damage and does not bring in mechanical residual stress damage. Besides the removal efficiency of ICPE is much higher than that of MRF. Therefore, these results demonstrate ICPE as a good post-process-

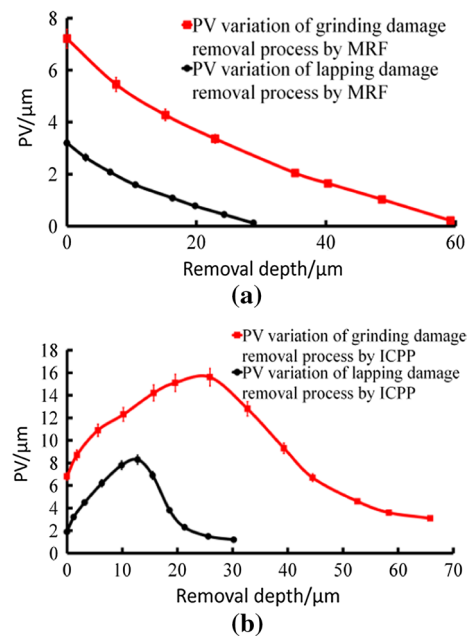


Fig. 15 PV value of the grinding and lapping surface at different removal depths: **a** MRF, and **b** ICPE

ing method for efficiently removing the grinding and lapping damage.

For further investigation of evolution of the grinding and lapping damage during ICPE process, the PSD analysis of experiment results (Figs. 13a, c, f, 14a, d, f) is carried out. The PSD curves are results of average profile. Figure 16a shows that the low spatial frequency (LSF, less than 0.021 mm^{-1}) errors increase obviously, whereas the middle-to-high spatial frequency (MHSF, 0.028 mm^{-1} to 0.51 mm^{-1}) errors firstly increase, and then decrease with the increase of removal depth. Figure 16b also shows that LSF (less than 0.035 mm^{-1}) errors increase finally, whereas the MHSF (0.046 mm^{-1} to 0.46 mm^{-1}) errors firstly increase, and then decrease with further processing. The analysis demonstrates that the spatial frequency errors firstly evolve to higher spatial frequency errors, and then evolve to lower frequency errors with iterative processing. Accordingly, the lateral and medial cracks firstly develop to fully-grown cracks (Figs. 3g, 10g, 11d), which results in the increase of the MHSF errors. Meanwhile, the fully-grown cracks extend to merge together (Figs. 3h–l, 10h–j, 11f, g), and then is gradually smoothed with further plasma etching, and thus leads to the process of MHSF errors evolving to LSF errors. It is obviously verified that the LSF errors increase rather than decrease finally as the cracks evolving to surface errors at larger scale (Figs. 2, 3, 4). After layer-by-layer removed by ICPE, the damage

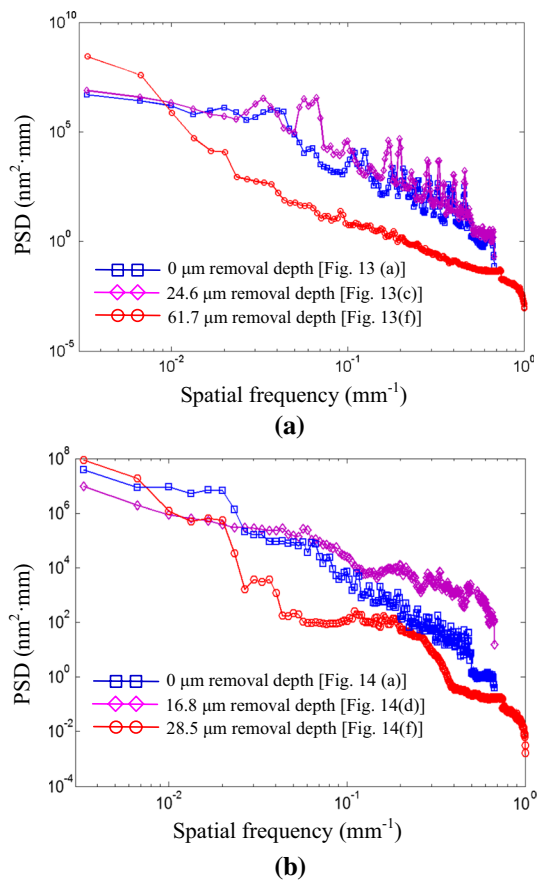


Fig. 16 Analysis of PSD during ICPE process: **a** ground surface and **b** lapped surface

microstructure is more obvious during the initial damage exposure, and the PV value becomes larger, so that the PV value of the surface also becomes larger, and the errors increase on the whole spatial frequency. Then the damage is removed through the brittle scratches, lateral and medial cracks merge together and form larger scale surface errors. These surface errors lead to increase of LSF. Therefore, PSD analysis demonstrates the morphology evolution process of the grinding and lapping damage during ICPE process.

- (3) Efficient processing of ground and lapped surface by ICPE. Experiment results demonstrate that efficient processing of ground and lapped surface needs to choose the appropriate parameters of ICPE based on the severity of surface damage. When the processing parameters are chosen, the removal depth is determined. If a parameter with a low removal rate is selected to process the severe damage surface such as the ground surface, the processing efficiency will decrease. If a parameter with a high removal rate is selected to treat slight damage surface such as lapped surface, the surface form accuracy is difficult to be

maintained. Therefore, the appropriate processing parameter should be applied to the damage distribution of different degree through the relationship between MRR and plasma scanning rate [26]. Thus, our optimized process of efficient damage removal by ICPE can be concluded as follows: Firstly, The maximum damage depths and the damage distribution should be detected (Figs. 10, 11). Secondly, the appropriate processing parameters of ICPE should be selected (If the high-precision surface form is required, the surface figuring method for compensating the thermal effect must be considered) [15, 25, 26]; Thirdly, Perform iterative processing until the damage is removed.

7 Conclusion

In this paper, the damage surface evolution during ICPE process is studied. The conclusions are as follows:

- (1) Scratch damage removal results reveal that the brittle scratch damage is successfully smoothed. Meanwhile the lateral and medial cracks around the scratch are gradually exposed, and then eliminated by ICPE.
- (2) The exposure of the lateral and medial cracks on the ground and lapped surface causes the increase of surface error during ICPE process. Moreover, the instinctive fused silica surface without the mechanical contact residual stress could be acquired through the chemical etching. Therefore, ICPE could be a good post-processing method for efficiently removing the grinding and lapping damage of fused silica.
- (3) The ground and lapped surfaces with a size of $300 \times 300 \times 20 \text{ mm}^3$ are efficiently processed by ICPE, respectively. PSD analysis further demonstrates the damage morphology evolution of the ground and lapped surfaces during ICPE process. It provides guidance for optimizing the grinding and lapping damage removal processes to efficiently improve surface quality, precision and fabrication efficiency of fused silica optics. In future research, the thermal effect of ICPE should be considered for achieving high-accuracy of larger fused silica surface.

Acknowledgements This research work was supported by Natural Science Foundation of China (51835013, U1801259), Natural Science Foundation of Hunan Province (2017JJ1004).

References

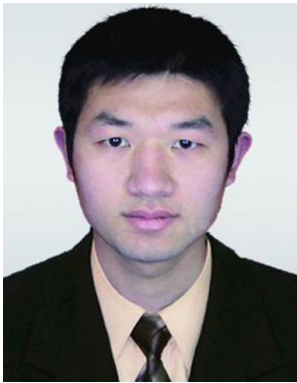
- Shen, N., Bude, J. D., & Carr, C. W. (2014). Model laser damage precursors for high quality optical materials. *Optics Express*, 22(3), 3393–3404.
- Wang, Z., Wu, Y., Dai, Y., & Li, S. (2008). Subsurface damage distribution in the lapping process. *Applied Optics*, 47(10), 1417–1426.
- Menapace, J. A. (2010). Developing magnetorheological finishing (MRF) technology for the manufacture of large-aperture optics in megajoule class laser systems. Office of Scientific and Technical Information Technical Reports 7842 (pp. 78421W–78421W-15).
- Bude, J., Miller, P., Baxamusa, S., Shen, N., Laurence, T., Steele, W., et al. (2014). High fluence laser damage precursors and their mitigation in fused silica. *Optics Express*, 22(5), 5839–5851.
- Miller, P. E., Suratwala, T. I., Bude, J. D., Laurence, T. A., Shen, N., Steele, W. A., et al. (2009). Laser damage precursors in fused silica. *Proceedings of SPIE*, 7504, 75040X.
- Menapace, J., Penetrante, B., Golini, D., Slomba, A., Miller, P., Parham, T., et al. (2002). Combined advanced finishing and UV-Laser conditioning for producing UV-damage-resistant fused silica optics. *Proceedings of SPIE*, 4679, 56–68.
- Liu, H., Ye, X., Zhou, X., Huang, J., Wang, F., Zhou, X., et al. (2014). Subsurface defects characterization and laser damage performance of fused silica optics during HF-etched process. *Optical Materials*, 36, 855–860.
- Néauport, J., Ambard, C., Cormont, P., Darbois, N., Destribats, J., Luitot, C., et al. (2009). Subsurface damage measurement of ground fused silica parts by HF etching techniques. *Optics Express*, 17(22), 20448–20456.
- Xu, M., Dai, Y., Zhou, L., Shi, F., Wan, W., Xie, X., et al. (2016). Investigation of surface characteristics evolution and laser damage performance of fused silica during ion-beam sputtering. *Optical Materials*, 58, 151–157.
- Shi, F., Zhong, Y., Dai, Y., Peng, X., Xu, M., & Sui, T. (2016). Investigation of surface damage precursor evolutions and laser-induced damage threshold improvement mechanism during Ion beam etching of fused silica. *Optics Express*, 24(18), 20842–20854.
- Kamimura, T., Akamatsu, S., Yamamoto, M., Yamato, I., Shiba, H., Motokoshi, S., et al. (2003). Enhancement of surface-damage resistance by removing a subsurface damage in fused silica. *Proceedings of SPIE*, 5273, 244–249.
- Xu, M., Shi, F., Zhou, L., Dai, Y., Peng, X., & Liao, W. (2017). Investigation of laser-induced damage threshold improvement mechanism during ion beam sputtering of fused silica. *Optics Express*, 25(23), 29260–29271.
- Fanara, C., Shore, P., Nicholls, J. R., Lyford, N., Kelley, J., Carr, J., et al. (2006). A new reactive atom plasma technology (RAPT) For precision machining: the etching of ULE surfaces. *Advanced Engineering Materials*, 8(10), 933–939.
- Jourdain, R., Castelli, M., Shore, P., Sommer, P., & Proscia, D. (2013). Reactive atom plasma (RAP) figuring machine for meter class optical surfaces. *Precision Engineering*, 7(6), 665–673.
- Shi, B., Dai, Y., Xie, X., Li, S., & Zhou, L. (2016). Arc-enhanced plasma machining technology for high efficiency machining of silicon carbide. *Plasma Chemistry and Plasma Processing*, 36(3), 1–10.
- Arnold, T., Böhm, G., Fechner, R., Meister, J., Frost, F., Hänsel, T., et al. (2010). Ultra-precision surface finishing by ion beam and plasma jet techniques—status and outlook. *Nuclear Instruments and Methods in Physics Research*, 616(2–3), 147–156.
- Meister, J., & Arnold, T. (2011). New process simulation procedure for high-rate plasma jet machining. *Plasma Chemistry and Plasma Processing*, 31(1), 91–107.
- Arnold, T., & Böhm, G. (2012). Application of atmospheric plasma jet machining (PJM) for effective surface figuring of SiC. *Precision Engineering*, 36(4), 546–553.
- Arnold, T., Böhm, G., & Paetzelt, H. (2016). Nonconventional ultra-precision manufacturing of ULE mirror surfaces using atmospheric reactive plasma jets. *Proceedings of SPIE*, 9912, 99123N.
- Castelli, M., Jourdain, R., Morantz, P., & Shore, P. (2012). Rapid optical surface figuring using reactive atom plasma. *Precision Engineering*, 36(3), 467–476.
- Zhang, J., Li, B., Wang, B., & Dong, S. (2013). Analysis on formation mechanism of ultra-smooth surfaces in atmospheric pressure plasma polishing. *International Journal of Advanced Manufacturing Technology*, 65(9–12), 1239–1245.
- Li, S., Wang, Z., & Wu, Y. (2008). Relationship between subsurface damage and surface roughness of optical materials in grinding and lapping processes. *Journal of Materials Processing Technology*, 205(1), 34–41.
- Ren, K., Luo, X., Zheng, L., Bai, Y., Li, L., Hu, H., et al. (2014). Belt-MRF for large aperture mirrors. *Optics Express*, 22(16), 19262–19276.
- Cheng, H. B., Feng, Z. J., & Wang, Y. W. (2005). Surface roughness and material-removal rate with magnetorheological finishing without subsurface damage of the surface. *Journal of Optical Technology*, 72(11), 865–871.
- Chen, H., Zhou, L., Xie, X., Shi, B., & Xiong, H. (2016). Rapidly removing grinding damage layer on fused silica by inductively coupled plasma processing. *Proceedings of SPIE*, 9683, 96830B.
- Dai, Z., Xie, X., Chen, H., & Zhou, L. (2018). Non-linear compensated dwell time for efficient fused silica surface figuring using inductively coupled plasma. *Plasma Chemistry and Plasma Processing*, 38(2), 443–459.
- Xin, Q., Li, N., Wang, J., Wang, B., Li, G., Ding, F., et al. (2015). Surface roughening of ground fused silica processed by atmospheric inductively coupled plasma. *Applied Surface Science*, 341, 142–148.
- Xin, Q., Su, X., & Wang, B. (2016). Modeling study on the surface morphology evolution during removing the optics surface/subsurface damage using atmospheric pressure plasma processing. *Applied Surface Science*, 382, 260–267.
- Takino, H., Yamamura, K., Sano, Y., & Mori, Y. (2010). Removal characteristics of plasma chemical vaporization machining with a pipe electrode for optical fabrication. *Applied Optics*, 49(23), 4434.
- Oh, C., Kang, M., & Hahn, J. W. (2015). Accurate measurement of atomic chlorine radical density in process plasma with spatially resolvable optical emission spectrometer. *International Journal of Precision Engineering and Manufacturing*, 16(9), 1919–1924.
- Sung, S., Kim, C. H., Lee, J., Jung, J. Y., Jeong, J., Choi, J. H., et al. (2014). Advanced metal lift-offs and nanoimprint for

- plasmonic metal patterns. *International Journal of Precision Engineering and Manufacturing-Green Technology*, 1(1), 25–30.
32. Lee, H., Chung, M., Ahn, H. G., Kim, S. J., Park, Y. K., & Jung, S. C. (2015). Effect of the surfactant on size of nickel nanoparticles generated by liquid-phase plasma method. *International Journal of Precision Engineering and Manufacturing*, 16(7), 1305–1310.
33. Lian, Y. S., Chen, H. F., & Mu, C. L. (2019). Performance of microtextured tools fabricated by inductively coupled plasma etching in dry cutting tests on medium carbon steel workpieces. *International Journal of Precision Engineering and Manufacturing-Green Technology*, 6(2), 175–188.

Publisher's Note Springer Nature remains neutral with regard to jurisdictional claims in published maps and institutional affiliations.



Xuhui Xie received PhD degree in mechanical engineering from National University of Defense Technology (NUDT). He is a professor in Mechanical Engineering at NUDT, China. His current research interests focus on ion beam figuring (IBF) and optical precision machining. Email: xuhuixie67@sina.com



Zuocai Dai is a PhD candidate in mechanical engineering from National University of Defense Technology (NUDT), China. His current research interests focus on inductively coupled plasma processing (ICPP) and optical precision fabrication. Email: daizuocai@163.com



Lin Zhou received his PhD degree in mechanical engineering from National University of Defense Technology (NUDT) in 2008. He is currently a professor in Mechanical Engineering at NUDT, China. His current research interests focus on ion beam figuring (IBF) and optical precision fabrication. Email: zhoulin9013@gmail.com



Shanyong Chen received PhD degree in mechanical engineering from National University of Defense Technology (NUDT) in 2006. He is currently a professor in Mechanical Engineering at NUDT, China. His current research interests focus on optical testing and ultra-precision machining. Email: mesy-chen@163.com